MACHINING OF UD - CFRP COMPOSITES: EXPERIMENTS AND FINITE ELEMENT MODELING

G. Venu Gopala Rao[1], Puneet Mahajan[1] and Naresh Bhatnagar[2, *]
[1]*Department of Applied Mechanics,*
[2]*Department of Mechanical Engineering,*
Indian Institute of Technology Delhi, New Delhi-110016, India
*E-mail: nareshb@mech.iitd.ernet.in

ABSTRACT

Spectrum of the study is to estimate the machining response of unidirectional carbon fiber reinforced plastic (UD-CFRP) composites. A single-phase macro-mechanical and two-phase micro-mechanical finite element (FE) model is used. The cutting and thrust forces during orthogonal machining were studied both experimentally and numerically for a range of fiber orientations, depths of cut and tool rake angles. Both cutting and thrust force measured from the micro-mechanical FE model matches well with the experiments, whereas cutting forces as measured from the macro-mechanical FE model matches well with the experiments, but the thrust force do not. The failure of fiber is found to be a combination of bending (from rear side) and crushing (from front side) for higher fiber orientation, while the bending effect becomes more significant for the lower fiber orientation.

Keywords: Carbon fiber, Composites, Machining, Finite Elements, Forces.

1. INTRODUCTION

Machining of UD-CFRP products is very complex, due to its material discontinuity, inhomogenity and anisotropic nature. Compared to the machining of metals, studies on machining of composites are few and limited in number. An experimental work on cutting of UD-CFRP composites was presented by *Koplev et al.* [1]. The machining characteristics were considered only for parallel and perpendicular fiber orientations and results were presented for chip size, cutting and thrust force variations with rake and relief angles. *Bhatnagar et al.* [2] ascribed fiber breakage due to axial tension as the cutting mechanism, which was also corroborated by *Wang* and *Zhang,* [3]. *Arola and Ramulu* [4] observed from experiments that both cutting and thrust force registered a minimum in the 15^o-30^o fiber orientation range and increases thereafter up to 90^o. Recently present authors, *Rao et al.* [5] proposed a new micro-mechanical FE model to estimate the chip formation mechanism in UD-GFRP composites. However, no such study has been done to estimate the machining response of UD-CFRP composites.

Objective of this article is to study the machining response experimentally as well as numerically for the range of fiber orientations (θ), depths of cut (t), tool rake angles (γ). The numerical study has been performed at two different scales, such as macro and micro-mechanical FE model. Initially the numerical studies were done at macro-scale and later on the study has been shifted to micro-model; this is due to certain shortcomings in the macro-model. In the macro-model both Tsai-Wu and critical stress failure criterion has been implemented to simulate the cutting process whereas in the micro-model matrix, interface and fiber failure is consider separately. The damage

initiation and evolution in the matrix is implemented based on the material yield strain and fracture energy respectively. Interface between the fiber and matrix were studied using cohesive zone model (CZM) (*Camanho* and *Dávila,* [6]). The contact pressures (p) at the cutting tool-work material interface, stresses in the fiber and matrix, their variation with fiber orientation, possible fracture mechanisms of the fiber, damage in the matrix, and interfacial debonding are also studied.

2. MACHINING EXPERIMENTS

UD-carbon fiber tapes, Epoxy (LY 556) along with hardener (HY 951) are used to prepare specimens. Orthogonal machining experiments for UD-CFRP laminates were performed on a vertical CNC milling machine (Beaver Mill NC-5). The tool geometry and process parameters are presented in **Table 1.** The specimen holder was mounted on a four-component piezoelectric dynamometer (KISTLER MODEL 9272), which in turn was clamped to the machine table. The chip formation mechanism was observed using a long-distance stereo zoom trinocular optical microscope (Zeiss). The microscope along with Charge coupled device (CCD) camera (SONY) was attached in series and used to view the magnified images of chip formation zone. **Figure 1 (a)** shows the schematic of the complete experimental set-up for both cutting and thrust force measurements and chip formation observations.

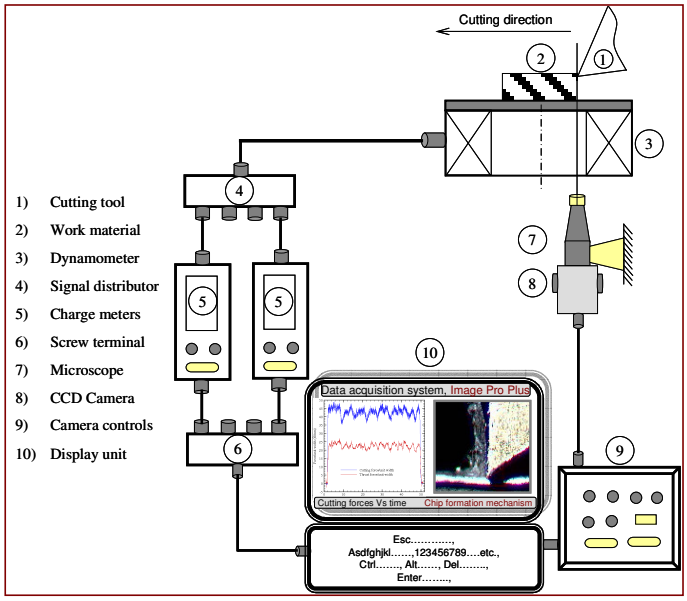

Figure 1. Schematic view of the experimental set-up.

3. FINITE ELEMENT FORMULATION

3.1 Macro-mechanical FE approach

In the present study, two different scale (macro and micro) finite element models are developed to estimate the response of the machining process and are discussed. Finite element method (FEM) is widely used to predict the machining response of metals and the same technique has been extended to composites. A plane stress finite element formulation with quasi-static option is used to study the machining of composites as explained by *Arola* and *Ramulu,* [4]. In the numerical model, to keep the problem tractable, only region of the work material close to chip formation zone is modeled (2000 µm x 1000 µm). The portion of the work material adjacent to the cutting tool is modeled to glide over the rake face. The schematic view of the macro-mechanical FE

model is shown in **Figure 2**. The mechanical properties of UD-CFRP composite were considered as EHM, where the fiber and matrix are replaced the equivalent homogeneous material. The mechanical stiffness properties of the UD-CFRP composites are measured from the in house experimentation and are then used in the numerical simulations as presented in **Table 2**. The normal tensile failure strengths for various off-axes are calculated from the strength transformation, whereas the in-plane shear strength properties for various off-axes are found from the Iosipescue shear test (*Walrath* and *Adams,* [7]).

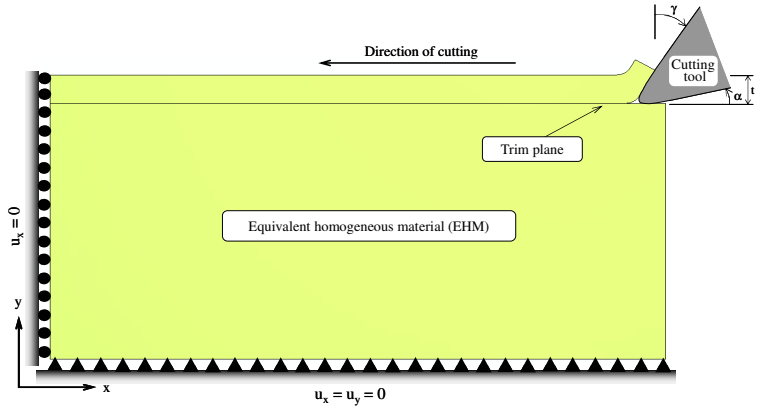

Figure 2. Schematic view of macro-mechanical FE model, where 't' is the depth of cut, 'γ' is the rake angle and 'α' is the relief angle.

The FE code has a provision for implementing node-debonding along the trim plane by critical stress failure criterion and also one can estimate the material damage during the machining process based on the Tsai-Wu failure criterion.

(a) Critical stress failure criterion

The induced stresses at the node nearest to the tool-tip is compared with a pre-defined critical stress, according to criterion stress factor 'f_{cri}'. The node separation is allowed when the state of stress at the node ahead of the cutting tool-tip exceeds a specified threshold value. The criterion stress factor, 'f_{cri}' can be expressed as:

$$f_{cri} = \sqrt{(\sigma_n / \sigma_f)^2 + (\tau_l / \tau_l^f)^2} \tag{1}$$

where, σ_n and σ_f are the normal tensile stress and failure strength at the node nearest to tool-tip respectively, similarly τ_l and τ_l^f are the shear stress and failure strength at the node nearest to the tool-tip respectively.

(b) Tsai-Wu failure criterion

Tsai-Wu failure criterion is used to estimate the material failure (*Herakovich,* [8]) ahead of the debonded node resulting in a chip. The chip formation and its subsequent release due to material failure are then allowed when the Tsai-Wu failure criterion ahead of the debonded node is achieved at the upper edge of the work-material. The Tsai-Wu failure criterion can be expressed as follows:

$$FI = F_1\sigma_{11} + F_2\sigma_{22} + F_{11}\sigma_{11}^2 + F_{22}\sigma_{22}^2 + F_{66}\tau_{12}^2 + 2F_{12}\sigma_{11}\sigma_{22} \tag{2}$$

$$F_1 = \frac{1}{X_t} + \frac{1}{X_c},\ F_2 = \frac{1}{Y_t} + \frac{1}{Y_c},\ F_{11} = -\frac{1}{X_t X_c},\ F_{22} = -\frac{1}{Y_t Y_c},\ F_{66} = \frac{1}{S_{xy}^2},\ F_{12} = f^* \sqrt{F_{11}F_{22}} \tag{3}$$

where 'FI' is the failure index, the material failure occurs when it reaches '1', with

$-1.0 \le f^* \le 1.0$. In the present study f^* is considered as zero. σ_{11}, σ_{22} and τ_{12} are the induced stresses in along, across and in-plane direction of the fiber respectively. X_t, Y_t are the tensile strength along and across the fiber similarly X_c, Y_c are the compressive strength along and across the fiber respectively. S_{xy} is the in-plane shear strength.

3.2 Micro-mechanical FE approach

Commercially available finite element analysis software tool ABAQUS^{TM} version 6.5 *Hibbit,* [9] is used for the present simulations. A plane stress FE formulation is used to study the machining of FRP composites. The portion of the work material adjacent to the cutting tool is modeled using fiber and matrix separately, whereas, portions away from the cutting tool are modeled as EHM. Two fibers, three matrix layers and two EHM regions as shown in **Figure 3** are considered in the present study.

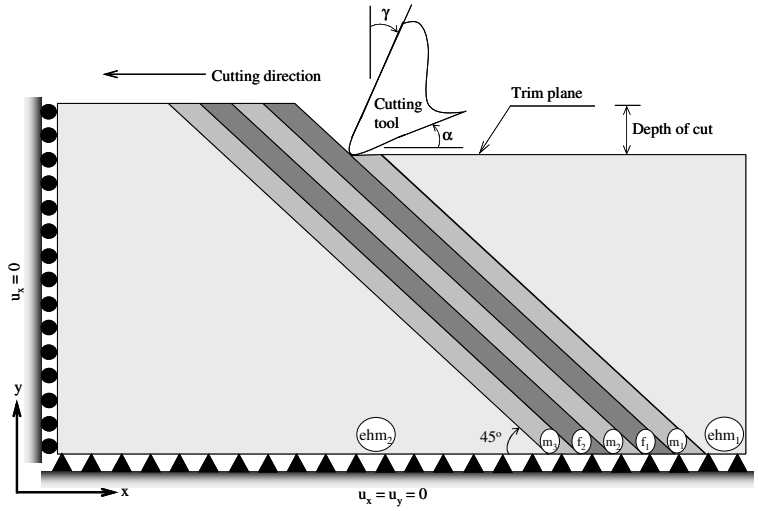

Figure 3. Schematic view of fiber (f_1 and f_2), matrix (m_1, m_2 and m_3) and EHM (ehm_1 and ehm_2) domains in the micro-mechanical FE model at 45^o fiber orientation, where 'γ' is the rake angle and 'α' is the relief angle.

The mechanical properties of fiber, matrix and interface are taken from the literature (*Kawabata,* [10]; *Kozey et al.,* [11]; *DiFrancia et al.,* [12]; *Meurs et al.,* [13]; and *Hobbiebrunken et al.,* [14]) and these properties are presented in the **Table 3**. The machining experiments show that the velocity of cutting marginally affects the cutting forces in composites. The FE code has provision for implementing damage initiation and evolution in matrix and debonding at the interface of fiber and matrix using cohesive elements.

(a) Damage initiation and evolution in the matrix material

The epoxy matrix exhibits elasto-plastic behavior *Hobbiebrunken et al.* [14]. Young's Modulus and Poisson's ratio characterize the linear elastic behavior. The von Mises yield criterion and isotropic hardening are used to define the plastic behavior of the epoxy matrix. This criterion predicts that yielding occurs when the elastic shear strain energy density reaches a critical value. The yielding is followed by hardening till a maximum strength is reached and subsequently it fails by strain softening due to onset of damage in the form of micro voids (or) micro cracks. The damage is considered

isotropic assuming that the micro cracks are initiated and propagated uniformly in all the directions. Since the damage does not depend on the direction, it can be completely characterized by a dimensionless scalar variable 'd_m'. The damaged modulus of elasticity 'E' can be related to the isotropic damage variable as

$$E = (1 - d_m)E_e \tag{4}$$

where, 'E_e' is the modulus of elasticity of the undamaged material point.

(b) Failure of the fiber material

Carbon fiber is assumed as an elastic and transverse isotropic. The elements in the fiber are considered failed once the principal stresses at the Gauss integration point reaches a critical value. The fiber element loses its load carrying capacity and its stiffness is slowly reduced to zero once the induced maximum principal stress reaches its failure strength of the fiber during the FE simulation.

(c) Cohesive zone modeling for the interfacial failure

Cohesive zone model (CZM) is a fracture mechanics approach to study the interfacial effects of either dissimilar material or in the same material when these are initially bonded together (*Camanho* and *Davila,* [6]). During the chip formation, the interfacial crack grows under the mixed mode loading. Therefore, a general formulation for cohesive elements dealing with mixed mode debonding is required. CZM approach has been used for debonding at fiber-matrix interface during orthogonal machining of UD-CFRP composites. The interfacial properties of the present material system are adapted for the literature (*DiFrancia et al.,* [12] and *Merus et al.,* [13]).

4. RESULTS AND DISCUSSION

4.1 Cutting and thrust forces analysis

In this section, the simulated cutting and thrust forces are compared with respective experimental observations. The variation of cutting and thrust forces (from experiments, macro-mechanics, micro-mechanics) with fiber orientation and depth of cut at 5° rake angle are presented in **Figure 4(a)** and **Figure 4(b)** respectively.

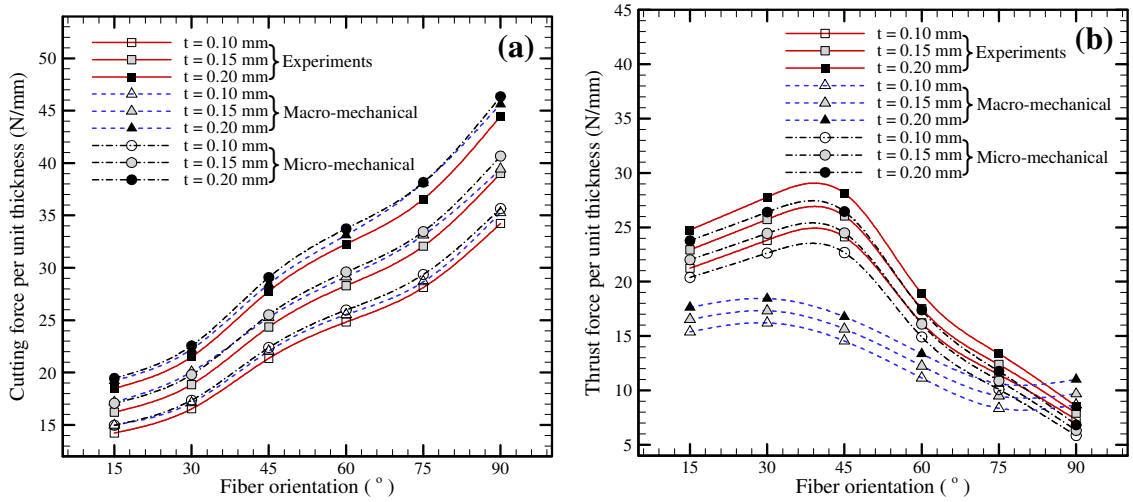

Figure 4. Variation of (a) cutting and (b) thrust forces with fiber orientation and depth of cut at γ=5° from the experiments, macro and micro-mechanical FE model.

From **Figure 4(a)**, it can be easily interpreted that; the predicted cutting forces from both macro and micro-model are always matching well with the experimental results.

However, the thrust found from the macro-model are does not matches well with experimental observations. The cutting forces found from the micro-model are higher than the experimental observations and the predicted thrust forces are always lower than the experimental observations. This is attributed to the 2-D representation of machining in FE simulation. In the simulations the tool only contacts the fiber whereas in reality it contacts both fiber and matrix simultaneously. The effective stiffness of combined fiber and matrix in real material is likely to be less than the individual stiffness of the fiber. The contact forces and therefore cutting force during the simulation are higher. The thrust forces in the simulation are low, because in the FE model the material is considered as virgin and the cutting tool is directly in contact with the trim plane. In the experiments, on the other hand, some uncut portion of the work material remains above the trim plane and the cutting tool has to travel over this uncut material to cut the next chip (*Wang* and *Zhang,* [3]). The force required to press this uncut portion, probably accounts for higher experimental values of thrust forces.

(a) Effect of fiber orientation

With an increase of fiber orientation, the cutting force increases almost linearly irrespective of depth of cut as shown in **Figure 4(a)**, as per the newly developed micro-mechanical FE model, the cutting and thrust forces are derived form the contact pressure and frictional shear stress. Cutting forces are continuously increases with fiber orientation irrespective of the depth of cut and rake angle. Thrust forces initially increases as fiber orientation increases from 15^{o} to 45^{o} and there after continuously decrease as shown in **Figure 4(a, b)**.

(b) Effect of depth of cut

The depth of cut is also a significant parameter in machining of UD-FRP composites. Both cutting and thrust forces increase with depth of cut as shown in **Figure 4(a, b)**. This is similar to the results of *Koplev et al*. [1], who report that cutting force and thrust force increase with depth of cut, but the cutting forces are more significant as compared to the thrust forces. The increase in these thrust forces is because of more force required to deform more material.

(c) Effect of tool rake angle

The effect of rake angle on both cutting and thrust forces is less significant as compared to the effect of fiber orientation and depth of cut. However, both the cutting and thrust forces decreases with rake angle in magnitude, the forces decrease is approximately 3% for every increment of 5^{o} rake angle. Similar trends were reported by many researchers (*Koplev et al.* [1]; and *Wang* and *Zhang*, [3]).

4.2 Chip formation mechanism

4.2.1 Experimental and simulation observations

Discontinuous chips are observed throughout the machining process, the process of the chip formation is due to failure of the interface, matrix cracking and fiber breaking that leads to discontinuous chip formation. Experiments also show that the size and shape of the chip depends entirely on the fiber orientation and depth of cut and to a lesser extent on the tool geometry. A typical flow of chip under an optical microscope is presented in detail in **Figure 5(a)**. Different stages (I, II, III, IV, V and VI) of chip blocks are marked in it. Each chip block consists of group of fibers bonded with some portion of matrix material. The matrix probably also has many cracks and debonding between the fiber and matrix also occurs but these are not clearly visible with the existing magnification

of the long range optical microscope. The chip block is formed based on the shear failure between the fiber bundle and the matrix material. For the case of 90^o fiber orientation the chip has to rotate about 75^o (for 15^o rake angle) towards the cutting direction before releasing the final block of chip from the parent material. The large rotation leads to high interfacial shear leading to debonding between fiber and matrix and crushing of matrix into powder with tensile failure of the interface as well as the matrix. For the case of 15^o fiber orientation the chip blocks gets released from the parent material without rotation (for 15^o rake angle). It is very difficult to see the cracks in the matrix and the nature of the fiber failure under existing optical microscope online during the machining process. To overcome this difficulty, the released chip was colleted on a double adhesive tape during the machining process and was observed under the scanning electron microscope (SEM). These observations are presented in **Figure 5(b)**; from all these figures it can be observed that, there are many cracks in the matrix material and also interfacial debonding between the fiber and matrix. **Figure 5(b)** shows the case of 75^o fiber orientation at 0.15 mm depth of cut, 5^o rake angle. It shows that series of chip blocks are formed due to matrix failure and interfacial failure.

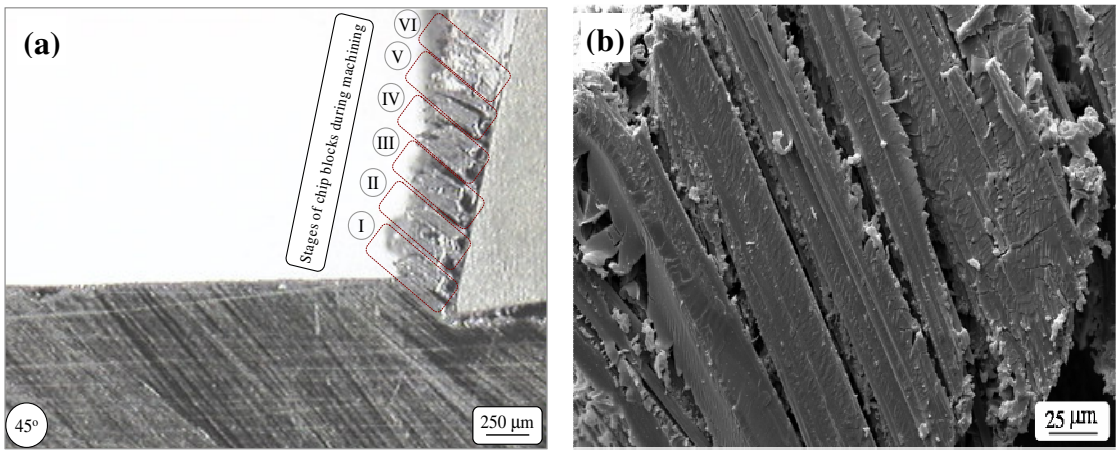

Figure 5. (a) Chip flow under an optical microscope for the case of 45^o fiber orientation. [I, II, III, IV, V, VI show the various stages of chip flow]. (b) SEM image of released chip for the case of 75^o fiber orientation at 0.15 mm depth of cut, 5^o rake angle.

From the numerical simulation, the variation of maximum principal stresses with depth of cut are presented in **Figure 6(a,b,c).** These stress contours are plotted at a constant rake angle of 5^o and fiber orientation of 45^o. From these figures one can conclude that, the stresses are high at the chip formation zone and local, which is true for all the depths of cut. However, for lower depth of cut the stresses reach the free surface of the work material and may help debonding from this location also.

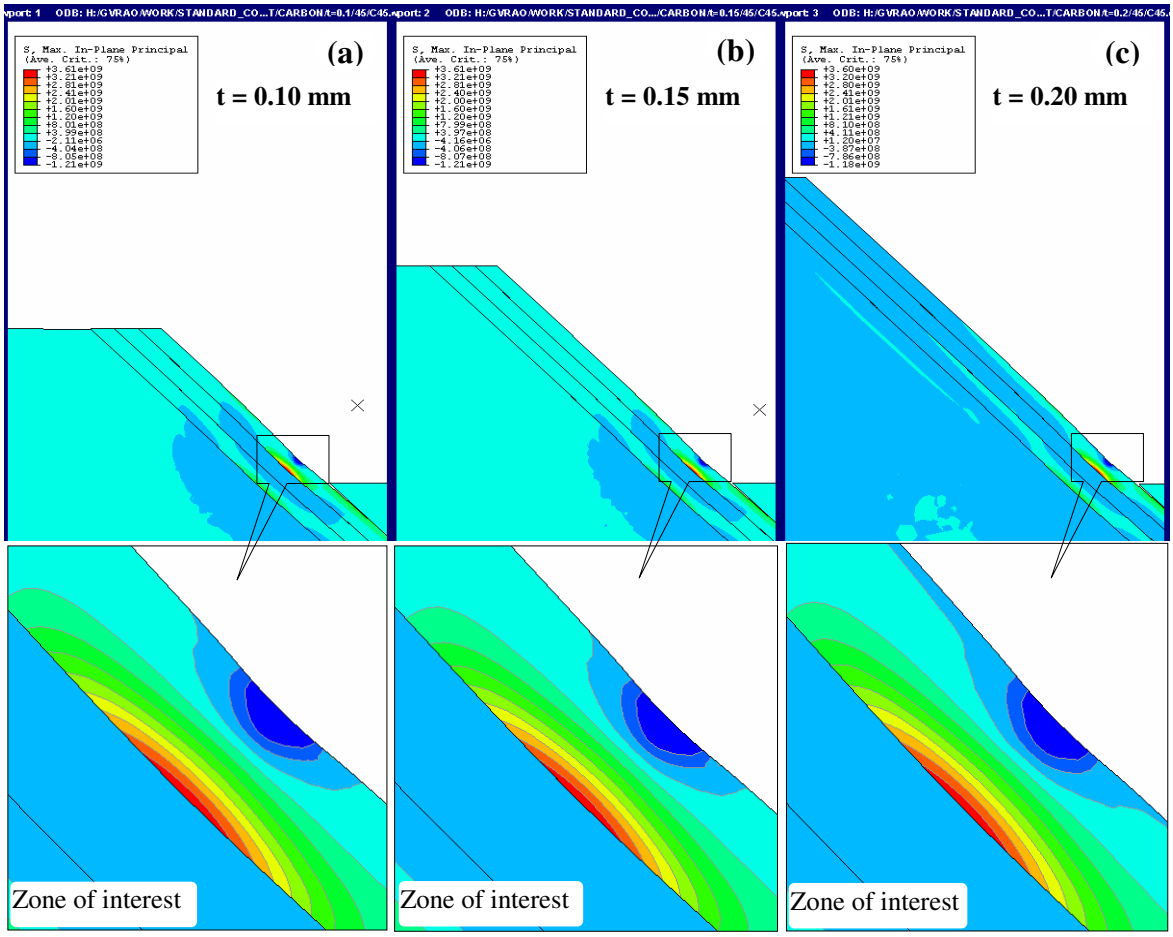

Figure 6. Contours of maximum principal stress in UD-CFRP composites at various depths of cut (a) t = 0.1, (b) t = 0.15 and (c) t = 0.2 mm at $\theta=45^{o}$, $\gamma=5^{o}$ [units of stresses, N/sq. m].

(a) Effect of fiber orientation

The observation of the chip formation mechanism is quite different for different fiber orientations. Powder like chip was observed in the higher fiber orientation, long chip was observed at lower fiber orientation. The shifting of contact zone is more for 15^{o} fiber orientation, and almost negligible for the case of 90^{o} fiber orientation. Due to the nature of Tsai-Wu stresses with change of fiber orientation, the chip formation and subsequent release gets effected.

(b) Effect of depth of cut

For a low depth of cut (0.1 mm) complete separation of fiber and matrix is observed, due to which powdery chip is also observed. For the case of 0.15 mm and 0.2 mm depth of cut the interfacial failure does not reach up to the free surfaces of the work material, due to which the size of the chip along the cutting direction is more and is measured to be 42 μm for 90^{o} and 68 μm for 15^{o} fiber orientation in UD-CFRP composites.

(c) Effect of tool rake angle

The effect of rake angle on the chip formation mechanism is marginal. For the case of fiber orientation between 15^{o} and 60^{o} there is absolutely no effect of rake angle. However, there is a slight influence of rake angle for the case of 75^{o} and 90^{o} fiber orientation. For these orientations before the release of the chip the parent material

directly touches the rake surface of the cutting tool. The chip failure progresses while the uncut material drags over the rake surface. For fiber orientations between 15^o and 60^o a complete chip failure take place before it can get dragged over the rake face.

5. SUMMARY AND CONCLUSIONS

Experimental and numerical investigations provide better understanding of the origin of cutting, thrust forces, chip formation mechanism. The single-phase macro-mechanical FE model gives reasonable estimation of cutting forces but thrust forces does not matches with experimental observations. The two-phase micro-mechanical FE model is a better representation of the UD-FRP composites for machining process as compared to an EHM model. The micro-mechanical FE study shows fiber, matrix and interfacial damage and possible locations of fiber breakage with subsequently release of blocky chip. For 90º fiber orientation both bending at fiber (f_1)-matrix (m_2) interface and crushing at cutting tool-fiber (f_1) interface causes fiber (f_1) fracture. As the orientation changes from 90º to 15º bending failure of the fiber becomes more significant. The cutting force mainly varies with fiber orientation and depth of cut and is very less dependent on rake angle.

REFERENCES

[1] Koplev A., Lystrup Aa., and Vorm T., "The cutting process, chips, and cutting forces in machining CFRP", *Composites*, 1983;14(4):371-376.

[2] Bhatnagar N., Ramakrishnan N., Naik N.K., and Komanduri R., "On the machining of fiber reinforced plastic (FRP) composite laminates", *Int J Mach Tools and Manufact*, 1995;35(5):701-716.

[3] Wang X.M., and Zhang L.C., "An experimental investigation into the orthogonal cutting of unidirectional fiber reinforced plastics", *Int J Mach Tools and Manufact*, 2003;43:1015-1022.

[4] Arola D., and Ramulu M., "Orthogonal cutting of fiber reinforced composites: A finite element analysis", *Int J Mech Sci*, 1997;39(5):597-613.

[5] Rao V.G., Mahajan P., and Bhatnagar N., "Machining of UD-GFRP Composites Chip formation mechanism", *Compos Sci Technol*, 2007; 67:2271-2281.

[6] Camanho P.P., and Dávila C.G., "Mixed-mode decohesion finite elements for the simulation of delamination in composite materials". NASA/TM-2002-211737, 2002:1-37.

[7] Walrath D.E., and Adams D.F., "The Iosipescu shear test as applied to composite materials". *Experimental Mechanics*, 1983;23(1):105-110.

[8] Herakovich C.T., "Mechanics of Fibrous Composites", John Wiley and Sons Inc., New York, 1998;316-319.

[9] Hibbit K.A.S., *Theory and User manuals V 6.5*, 2005;ABAQUS Inc. USA.

[10] Kawabata S., "Measurement of the Transverse Mechanical Properties of High-performance Fibers", *J. Text Inst,* 1990;81(4):432-447.

[11] Kozey V.V., Jiang H., Mehta V.R., and Satish K., "Compressive behavior of materials: Part II. High performance fibers". *J. Mater. Res.*1995;10(4):1044-1061.

[12] DiFrancia C., Ward Thomas C., and Claus Richard O., "The single-fiber pull-out test 1: Review and interpretation", *Compos Part A*, 1996;27A:597-612.

[13] Meurs P.F.M., Schrauwen B.A.G., Schreurs P.J.G., and Peijs T., "Determination of the interfacial normal strength using single fiber model composites", *Compos Part A*, 1998;29A:1027-1034,.
[14] Hobbiebrunken T., Fiedler B., Hojo M., Ochiai S., and Schulte K., "Microscopic yielding of CF/epoxy composites and the effect on the formation of thermal residual stresses". *Compos Sci and Technol,* 2005;65:1626-1635.

Table 1. Material, tool geometry and process parameters.

	Parameter	
UD-CFRP composites	Specimen dimensions	100 mm x 50 mm x 3 mm
Tool geometry parameters	Rake angle (γ)	5º, 10º and 15º
	Relief angle (α)	6º
	Edge radius (r)	50 μm
Process parameters	Depth of cut (t)	0.1, 0.15 and 0.2 mm
	Fiber orientation (θ)	15º, 30º, 45º, 60º, 75º & 90º
	Cutting speed (V)	0.5 m/min

Table 2. Stiffness and strength properties of UD-CFRP composites.

Stiffness properties				Strength properties				
E_1 (GPa)	E_2 (GPa)	G_{12} (GPa)	υ_{12}	X_t (MPa)	X_c (MPa)	Y_t (MPa)	Y_c (MPa)	S_{xy} (MPa)
139.4	9.5	5.8	0.24	1951	1475	47.1	188.4	74.28

Table 3. Stiffness and strength properties of fiber, matrix and interface.

Material	Property	
Carbon fiber	Elastic constants (Tension)	E_1 = 235 GPa, E_2 = 14 GPa, G_{12} = 28 GPa, υ_{12} = 0.2
	Elastic constants (Compression)	E_1 = 106 GPa, E_2 = 14 GPa, G_{12} = 28 GPa, υ_{12} = 0.2
	Tensile strength	Xt = 3.59 GPa, Yt = 0.35 GPa
	Compressive strength	X_c = 1.8 GPa, Y_c = 2.73 GPa
	Shear strength	S_{xy} = 0.38 GPa
Epoxy matrix	Elastic constant	E = 3.1 GPa, υ = 0.33
	Yield strength	σ_y = 27.5 MPa
	Tensile strength	σ_t = 70.3 MPa
	Fracture toughness	K_c = 0.5 MPa $m^{1/2}$
	Fracture energy	G_f = 80.6 J/m^2
Fiber-Matrix Interface	Normal strength	N = 167.5 MPa
	Shear strength	S = 21 MPa
	Fracture energy	G_{IC} = G_{IIC} = 50 N/m